DENND5A epileptic encephalopathy features global developmental delay, seizures and ventriculomegaly

Emily Banks[1], Fares Kharfallah[1], Vladimir Fonov[1], Armin Bayati[1], Vincent Francis[1], Gopinath Kulasekaran[1], Marius Tuznik[1], Chanshuai Han[1], Reem Al-Khater[2], Fowzan S. Alkuraya[3], Loukas Argyriou[4], Eileen Barr[5], Lauren Bartik[6,7], Miriam Bertrand[8], Rebecca Buchert[8], Maxime Cadieux-Dion[9], Heidi Cope[10], Donna Cushing[11], Thomas M. Durcan[1], Juanita Neira Fresneda[5], Tawfiq Froukh[12], Harinder K. Gill[13], Elaine Suk-Ying Goh[11], Tobias B. Haack[8], Mais O. Hashem[3], Stefan Hauser[14,15], Trevor L. Hoffman[16], Jacob S. Hogue[17], Stephanie Huynh[13], Silke Kaulfuß[4], G. Christoph Korenke[18], Amy Kritzer[19], Elysa J. Marco[20], Kirsty McWalter[21], Arakel Minassian[22], Berge A. Minassian[23], Hope Northrup[24], Barbara Oehl-Jaschkowitz[25], Matthew Osmond[26], Carol Saunders[6,9,27], Ludger Schoels[14,15], Undiagnosed Diseases Network[†], Dihong Zhou[6,7], Ziv Gan-Or[1,28], David A. Rudko[1], and Peter S. McPherson[1]

[†]The full list of authors in network is listed in Appendix 1.

Abstract

Epileptic encephalopathies comprise a clinically and genetically heterogenous group of disorders characterized by global developmental delay and ongoing seizure activity. It is generally considered that seizure activity is the primary pathology and leads to altered cognitive function. However, epileptic encephalopathy can also result from primary defects in neurodevelopment that lead to seizures. Here we examine the symptomology of individuals with epileptic encephalopathy resulting from biallelic pathogenic variants in *DENND5A*, encoding a protein involved in intracellular membrane trafficking.

We established a cohort of 15 individuals from 14 families with 21 unique variants in *DENND5A* and analyzed phenotypic surveys answered by their treating clinicians. We obtained cells derived from several cohort members and examined DENND5A expression and stability, and we

examined the role of DENND5A in symmetric cell division capability. Finally, we generated a mouse line expressing a homozygous mutation found in the cohort and analyzed brain morphology *in vivo* using a 7 Tesla magnetic resonance imaging system.

Our cohort study reveals that global developmental delay, gross abnormalities in brain development including ventriculomegaly and corpus callosum dysgenesis, seizures, microcephaly and hypotonia are found in the majority of the cohort. Patient-derived neural precursor cells from induced pluripotent stem cells, as well as patient-derived lymphoblasts, display loss of DENND5A protein and exhibit problems with symmetric cell division, an essential process in early neural development. The introduction of a homozygous human point mutation into the conserved sequence in mouse leads to an animal with reduced brain volume and widespread regional brain dysgenesis and ventriculomegaly, phenotypes shared with the human cohort. Taken together, our multi-dimensional study establishes *DENND5A* as a critical gene during neurodevelopment and that biallelic loss of function variants, including missense and truncating variants as well as intronic splice site variants, result in a developmental epileptic encephalopathy.

Author affiliations:

1 Department of Neurology and Neurosurgery, Montreal Neurological Institute, McGill University, Montréal, QC H3A 2B4, Canada

2 Johns Hopkins Aramco Healthcare, Dhahran 34465, Saudi Arabia

3 Department of Translational Genomics, Center for Genomic Medicine, King Faisal Specialist Hospital and Research Center, Riyadh 11564, Saudi Arabia

4 Institute of Human Genetics, University Medical Center, Göttingen 37073, Germany

5 Emory University, Department of Human Genetics, Atlanta, GA 30322, USA

6 University of Missouri-Kansas City, School of Medicine, Kansas City, MO 64108, USA

7 Department of Pediatrics, Division of Clinical Genetics, Children's Mercy Hospital, Kansas City, MO 64108, USA

8 Institute of Medical Genetics and Applied Genomics, University of Tübingen, Tübingen 72076, Germany

9 Department of Pathology and Laboratory Medicine, Children's Mercy Hospital, Kansas City, MO 64108, USA

10 Division of Medical Genetics, Department of Pediatrics, Duke University Medical Center, Durham, NC 27710, USA

11 Laboratory Medicine and Genetics, Trillium Health Partners, Mississauga, ON L5B 1B8, Canada

12 Department of Biotechnology and Genetic Engineering, Philadelphia University, Amman 19392, Jordan

13 Provincial Medical Genetics Program at BC Women's Health Centre, Vancouver, BC V6H 3N1, Canada

14 Center for Neurology and Hertie Institute for Clinical Brain Research, University Tübingen, Tübingen 72076, Germany

15 German Center of Neurodegenerative Diseases (DZNE), Tübingen 72076, Germany

16 Southern California Kaiser Permanente Medical Group, Department of Regional Genetics, Anaheim, CA 92806, USA

17 Madigan Army Medical Center, Tacoma, WA 98431, USA

18 Department of Neuropediatrics, University Children's Hospital, Klinikum Oldenburg, Oldenburg 26133, Germany

19 Division of Genetics and Genomics, Boston Children's Hospital, Boston, MA 02115, USA

20 Cortica Healthcare, San Rafael, CA 94903, USA

21 GeneDx, Gaithersburg, MD 20877, USA

22 Centre for Applied Genomics, Genetics, and Genome Biology, Hospital for Sick Children, Toronto, ON M5G 0A4, Canada

23 UT Southwestern Medical Center, Departments of Pediatrics and Neurology, Dallas, TX 75390, USA

24 Department of Pediatrics, McGovern Medical School at the University of Texas Health Science Center at Houston (UTHealth) and Children's Memorial Hermann Hospital, Houston, TX 77030, USA

25 Practice of Human Genetics, Homburg (Saar), Germany

26 Children's Hospital of Eastern Ontario Research Institute, University of Ottawa, Ottawa K1H 8L1, Canada

27 Center for Pediatric Genomic Medicine, Children's Mercy Hospital, Kansas City, MO 64108, USA

28 Department of Human Genetics, McGill University, Montréal, QC H3A 2B4, Canada

Correspondence to: Peter S. McPherson, PhD, FRSC

Distinguished James McGill Professor

Department of Neurology and Neurosurgery

Montreal Neurological Institute, McGill University

3801 University Street

Montreal, QC H3A 2B4

Canada

peter.mcpherson@mcgill.ca

Running title: DENND5A epileptic encephalopathy

Keywords: developmental delay; epilepsy; ventriculomegaly; neural precursor cells; autism spectrum disorder

Abbreviations: 7T = 7-Tesla; ASD = autism spectrum disorder; EE = Epileptic Encephalopathy; DENN = Differentially Expressed in Normal and Neoplastic cells; iPSC = induced pluripotent stem cell; H&E = hematoxylin and eosin; Mut = mutant; NPC = neural progenitor cell; PLAT = Polycystin-1, Lipoxygenase, Alpha-Toxin; RUN = RPIP8 [RaP2 interacting protein 8], UNC-14 and NESCA [new molecule containing SH3 at the carboxyl-terminus]; RARE = Rapid Imaging with Refocused Echoes; TORCH = Toxoplasmosis, Other agents, Rubella, Cytomegalovirus, and Herpes simplex; TR = repetition time; WT = wild-type

Introduction

Epileptic encephalopathies (EE) encompasses a broad range of conditions in which infants and children experience cognitive and behavioral decline as a result of ongoing seizure activity.[1] Genetic causes of EE typically involve genes coding for proteins that directly impact neuronal firing such as ion channels and neurotransmitter regulators.[2-4] In these cases, the seizures themselves are thought to damage cells and prevent proper neuronal development. However, evidence for the reverse scenario, in which compromised nervous system development is the primary issue with seizures occurring as a result of abnormal development, has also been established.[5] This dichotomy of disease etiology limits the scope of EE patient care to symptom management with questionable prognosis accuracy. Indeed, early detection and pharmaceutical intervention leads to better neurodevelopmental outcomes when the EE is primarily a seizure disorder,[2,6] but individuals in whom the EE is primarily a neurodevelopmental disorder may not have the same prognosis using the same interventions. Conversely, early behavioral interventions can significantly improve neurodevelopmental outcomes among individuals with congenital developmental disorders not primarily associated with seizure activity.[7,8] It is thus of utmost importance for clinicians to identify individuals in each category such that families will be given clear information regarding the most appropriate treatment recommendations and prognoses, and for the genetic forms, appropriate genetic counselling.

We previously described three individuals from two consanguineous families with a severe form of EE and homozygous variants in *DENND5A*. DENND5A protein is expressed prominently in the nervous system and its loss of function in neuronal cultures leads to altered neurite outgrowth.[9] DENND5A is a member of a family of minimally 25 proteins bearing a differentially expressed in normal and neoplastic cells (DENN) domain.[10,11] Via the DENN domain, the majority of these proteins function as guanine-nucleotide exchange factors (activators) of Rab GTPases, master regulators of membrane trafficking.[10,12] In addition to the DENN domain, DENND5A has two RUN (RPIP8 [RaP2 interacting protein 8], UNC-14 and NESCA [new molecule containing SH3 at the carboxyl-terminus]) domains. RUN domains are protein modules often associated with GTPases in the Rap and Rab families.[13] Through the most N-terminal RUN domain, DENND5A interacts with Rab6, giving DENND5A the basis for its original name of Rab6-interacting protein 1 (RAB6IP1).[14-16] Through the more C-terminal RUN

domain, DENND5A interacts with sorting nexin 1, a protein involved in protein trafficking between endosomes and the trans-Golgi network.[17,18] No specific protein interaction or other function has been observed with the PLAT domain (Polycystin-1, Lipoxygenase, Alpha-Toxin) of DENND5A, a little-studied beta sheet protein module involved in protein-protein and protein-lipid interactions.[19] Full-length DENND5A also interacts with GTP-Rab11, but no specific binding site has been identified.[20] The domain structure and protein partners of DENND5A suggest its involvement in intracellular membrane trafficking pathways, but these pathways yet to be identified.

Here, through physician-initiated contact and searching of disease variant databases, we identify a cohort of 15 individuals from 14 families with 21 unique *DENND5A* variants. Treating clinicians completed detailed anonymized phenotypic questionnaires relating to the individuals in their care. Analysis of compiled questionnaire data revealed that the seven homozygous recessive and eight compound heterozygous individuals exhibit the same cluster of developmental phenotypes, namely: global developmental delay, seizures, ventriculomegaly, hypotonia, reduced corpus callosum volume, and microcephaly. Although most cohort members exhibit severe phenotypes, some *DENND5A* variants appear to result in milder developmental outcomes, suggesting that some variants may have inherently more severe functional consequences than others.

This detailed analysis of the cohort, along with cell biological analysis of the variants and the development of a mouse model expressing a homozygous recessive variant from our proband patient, addresses our objective to demonstrate whether a causal link exists between biallelic pathogenic *DENND5A* variants and neurodevelopmental disease. Our results strongly support a causal relationship and will aid medical professionals by: a) streamlining the identification of new patients based on hallmark clinical features; b) encouraging the inclusion of *DENND5A* in genetic testing panels as a candidate gene for developmental disorders, especially those featuring the hallmarks of *DENND5A*-related EE; and c) providing families with more accurate prognostic information and treatment recommendations.

Materials and methods

Clinical data collection and analysis

Ethical approval

All materials and methods for participant recruitment and clinical data collection was approved by the McGill University Health Centre research ethics board (study 2021-6324) and the McGill Faculty of Medicine and Health Sciences institutional review board (study A12-M66-21B).

Recruitment

We originally identified four individuals, one deceased, from two consanguineous families with homozygous *DENND5A* variants.[9] Another two homozygous individuals were described by Anazi *et al*. in 2017.[21] Neither study provided a detailed phenotypic analysis. Here we identified an additional 13 individuals: five were brought to our attention by physicians who had performed diagnostic whole exome sequencing on patients and discovered *DENND5A* variants; five were identified through physician-submitted GeneMatcher[22] and ClinVar[23] database entries who performed whole-exome sequencing for similar clinical purposes; and another three were identified through word-of-mouth of the study between clinicians that already completed the survey and their colleagues with other *DENND5A* EE patients. Participant recruitment spanned approximately two years. Four individuals were excluded from the cohort and subsequent analysis: two were excluded due to not meeting eligibility criteria (both are heterozygous for a *DENND5A* variant, having only one affected allele); one was excluded due to death occurring prior to clinical data collection[9]; and one was excluded because the clinician did not return the questionnaire.

Phenotypic data collection and analysis

We devised a phenotypic questionnaire for physicians and genetic counselors to complete regarding their patients with *DENND5A* variants. A blank questionnaire is included in Supplementary Fig. 1.

Clinicians with patients harboring *DENND5A* variants of unknown or likely pathogenicity completed the anonymized phenotypic questionnaire based on their patient's most recent clinic

visit and contributed anonymized MRIs and/or or official reports if the patient underwent neuroimaging for clinical purposes. All clinicians reported phenotypes independent of the answers from other clinicians. Potential confounding variables include variants of unknown or likely pathogenicity in genes other than DENND5A and were also reported. Participants were assigned a numerical ID in the order in which their corresponding questionnaires were received.

Data are missing if the presence of a clinical phenotype is officially unknown. However, due to the small cohort size, statistical analyses were not performed and missing data did not greatly affect the study. Data were aggregated and the sum and/or percentage of cohort members exhibiting a given phenotype are reported. In instances where data are continuous, an average value is reported.

In vitro experiments

Establishment of patient-derived cell lines

The control induced pluripotent stem cell (iPSC) line AIW001-02 was derived from peripheral blood mononuclear cells of a healthy female donor (Caucasian, 48 years old). The AIW001-02 cell line was generated by using the CytoTune™-iPS 2.0 Sendai Reprogramming Kit (iPSQuebec Platform, Laval University). For knockout expression of human *DENND5A*, guide RNAs (gRNAs) were designed using an online tool (https://benchling.com). Both gRNA target sites are on *DENND5A* exon 4. Synthesized gRNAs were ordered from SYNTHEGO and transfection was performed following the manufacturer's protocol. Single cell colonies were picked and amplified. Genomic DNA from the colonies was extracted with QuickExtract (Lucigen) and PCR was performed using Q5 High-Fidelity DNA Polymerase according to the manufacturer's protocol (F: GAGGATCGCCAGTGAGTGTT; R: CCCCGAGCAGTTCAAAAACC). A 238 base pair deletion was confirmed by Sanger sequencing.

Human fibroblasts from DENND5A cohort members were obtained by skin biopsy and reprogrammed to iPSCs by electroporation of fibroblasts with episomal plasmids (pCXLE-hUL, pCXLE-hSK, and pCXLE-hOCT4) as previously described.[24] Generated iPSCs were functionally and genomically validated according to Hauser and Erzler.[25]

Lymphoblasts were obtained from a healthy individual (control line) and two homozygous patients. Cells were immortalized through use of the Epstein-Barr virus and generated in the lab of Dr. Fowzan Alkuraya.

iPSC culture and differentiation

iPSCs were cultured on hESC-qualified Corning Matrigel-coated tissue culture dishes in either TeSR-E8 medium (all patient-derived cell lines; STEMCELL Technologies) or mTeSR1 medium (AIW001-02 WT and AIW001-02 DENND5A KO; STEMCELL Technologies) with daily medium changes and mechanical removal of differentiated cells. Cells were passaged using the ReLeSR Passaging Reagent (STEMCELL Technologies) once cultures reached 70-90% confluency.

iPSCs were differentiated to neural progenitor cells (NPCs) using the STEMdiff SMADi Neural Induction Kit (STEMCELL Technologies) with daily medium changes. Induced cultures were passaged using Accumax (Millipore Sigma) once cells reached 90-95% confluency, approximately once per week. After a two-week induction period, NPCs were maintained in STEMdiff Neural Progenitor Medium (STEMCELL Technologies) on Matrigel-coated plates and passaged using Accumax at a 1:2-1:5 ratio once cultures reached 80-95% confluency.

Lymphoblastoid cell line culture

Control and patient-derived Epstein-Barr virus-induced lymphoblastoid cell lines were obtained from the laboratory of Dr. Alkuraya. Cells were cultured in suspension in RPMI 1640 medium (Gibco) supplemented with 15% fetal bovine serum (Wisent), 1% penicillin-streptomycin (Wisent), and 1% L-glutamine (Wisent). Cells were split 1:4 once confluency reached approximately 1 x 10^6 cells/ml.

Neurosphere formation assay

50 NPCs per well of each condition were seeded into an uncoated 96-well dish with six replicates per experiment. 50 µl media was added every 3-4 days, and 4X images were taken of the top, bottom, left, right, and middle of each well after 2 weeks in culture using the EVOS FLc microscope. Neurospheres at least 50 µm in diameter were identified using ImageJ. Data did not meet assumptions for ANOVA statistical testing, therefore the total number of spheres per well

were analyzed using Kruskal-Wallis one-way analysis of variance and Mann-Whitney U post-hoc statistical tests using Bonferroni corrections for multiple comparisons.

Endogenous DENND5A protein expression

NPCs and lymphoblasts were harvested in 20 mM HEPES pH 7.4, 100 mM NaCl, 0.83 mM benzamidine, 0.5 µg/ml aprotinin, 0.5 g/ml leupeptin, 0.23 mM phenylmethylsulfonyl fluoride, and 1X Lammeli sample buffer containing SDS. Equal whole-cell protein aliquots were loaded onto an SDS-PAGE gel and analyzed via Western blot using a primary antibody against DENND5A (ThermoFisher #702789, 2.5 µg/ml).

FLAG-DENND5A protein expression

HEK293-T cells were cultured in DMEM high glucose (Fisher) supplemented with 10% bovine calf serum (Fisher), 1% L-glutamine (Wisent), and 1% penicillin-streptomycin (Wisent). *DENND5A* cDNA (Origene, SC121400) was cloned into the pCMV-tag2B vector. Patient mutations were introduced using the QuikChange Lightning site-directed mutagenesis kit (Agilent) following the manufacturer's protocol. All constructs were confirmed by Sanger sequencing. Plasmid DNA was transfected using the calcium phosphate method and cells were harvested after 24 hours (20 mM HEPES pH 7.4, 100 mM NaCl, 0.83 mM benzamidine, 0.5 µg/ml aprotinin, 0.5 µg/ml leupeptin, 0.23 mM phenylmethylsulfonyl fluoride, and 1X Lammeli sample buffer containing SDS). Equal whole-cell protein aliquots were loaded onto an SDS-PAGE gel and analyzed via Western blot using primary antibodies against FLAG (clone M2, Sigma-Aldrich, 1:10,000).

RT-qPCR

RNA was extracted from NPCs and lymphocytes using the RNeasy kit (Qiagen), followed by cDNA synthesis using iScript Reverse Transcription Supermix for RT-qPCR (Bio-Rad). RT-qPCR was performed using SsoFast EvaGreen Supermix (Bio-Rad) with primers targeting human *DENND5A* (F: CTAAAGCCAGGGATGGTGCC; R: TTTCGGCATACATAGCATTCCT) and *TBP* (F: TGCACAGGAGCCAAGAGTGAA; R: CACATCACAGCTCCCCACCA). DENND5A levels were normalized to TBP levels and results were analyzed via one-way ANOVA and Tukey's post-hoc tests.

RNA from mouse brain tissue was extracted using RNeasy Lipid Tissue kit (Qiagen), followed by cDNA synthesis and RT-qPCR performed with the same reagents as above, but with primers specific to the mouse genome for *DENND5A* (F: CAGTCGCTTCGCCGACTAT; R: GCACCATCCCTGGCTTTAGAA) and *GAPDH* (F: ACTCCACTCACGGCAAATTC; R: CCAGTAGACTCCACGACATACT).

Animal experiments

Animal care and selection

All animal care and experiments in the study were approved by the Montreal Neurological Institute Animal Care Committee in accordance with guidelines set by the Canadian Council on Animal Care under ethical protocol number 5734. The experimental unit for this study is a single animal. Apart from selecting animals based on *DENND5A* genotype, no exclusion criteria were set for the experiments. No experimental confounders were anticipated and therefore were not controlled.

Establishment of transgenic mouse model

Mice were generated by the McGill Integrated Core for Animal Modeling. Two silent mutations were introduced in L168 and L169 (CTTGCT –> TTAGCA) as well as a deletion of 2 bp in G172 to introduce a frameshift and premature stop codon in exon 4 of the *DENND5A* mouse gene. Briefly, custom sgRNAs (Synthego), Cas9 protein (IDT, Cat# 1081058) and ssODN (ultramer, IDT) were microinjected into the pronucleus of C57BL/6N mouse zygotes with concentrations of 50:50:30 ng/µl respectively. Embryos were subsequently implanted in CD-1 pseudopregnant surrogate mothers according to standard procedures approved by the McGill University Animal Care Committee. Founder pups (F0) were genotyped for evidence of a deletion of 2 bp in G172 and mated to wild-type C57BL/6N (Charles River) mice for three generations. The colony was maintained by sibling mating and by crosses to C57BL/6N mice every third generation. All genomic sequencing was performed using the Big Dye Terminator Ready Reaction Mix (ABI, Carlsbad, CA, USA) at the McGill and Genome Quebec Innovation Center (Primers ACAAGGAATGCTCTCACTGC, CACACTCCGACATGCCTTCAT [417 bp]). Obtained sequences were analyzed using an online tool (https://benchling.com).

Endogenous DENND5A expression

Three E18 animals per experiment (one WT, one heterozygous, and one mutant) were used to examine DENND5A protein expression in multiple independent experiments. Brains were homogenized in lysis buffer containing 20 mM HEPES pH 7.4, 100 mM NaCl, 0.83 mM benzamidine, 0.5 µg/ml aprotinin, 0.5 µg/ml leupeptin, 0.23 mM phenylmethylsulfonyl fluoride, and 1% Triton. Insoluble material was removed by centrifugation and equal protein aliquots were loaded onto an SDS-PAGE gel and analyzed via Western blot using primary antibodies against DENND5A (ThermoFisher #702789, 2.5 µg/ml) and β-actin. The same researcher genotyped animals and performed the experiments.

Hematoxylin and eosin (H&E) staining

After deep anesthesia with isoflurane (Fresenius Kabi Canada), three adult mice per experiment (one WT, one heterozygous, and one mutant) were transcardially perfused with cold 4% paraformaldehyde (0.1 M NaPO4, pH 7.4). Brains were removed and fixed in buffer overnight at 4°C and subsequently embedded in paraffin and cut into sections with a 4 µm thickness. All H&E staining was performed using a standard protocol and imaged using the Nikon E800 microscope. Each experiment was repeated several times. The same researcher genotyped the animals and performed the experiments.

Small animal MRI

Eight WT (n = 8, five females, three males, mean age = 101 days, SD = 39.7) and eight homozygous mutant (n = 8, five females, three males, mean age = 95.2 days, SD = 34.8) for a total of 16 animals were employed for high resolution, pre-clinical MR imaging experiments. Data from one WT animal were excluded as part of a pilot study. For *in vivo* structural MRI, mice were anesthetized with isoflurane, placed in a plastic bed and restrained with gauze pads to minimize the possible influence of motion artifacts. For the duration of each MRI scan, mice were maintained under isoflurane gas anesthesia at approximately 37°C using a warm air blower and respiration was monitored using a pressure pad.

Imaging was performed using the 7 T Bruker Pharmascan (Bruker Biosciences, Billerica, MA), ultra-high field, pre-clinical MRI system of the McConnell Brain Imaging Centre at McGill University. The Pharmascan is equipped with an AVANCE II-model spectrometer and BFG-150/90-S shielded gradient system (Resonance Research Inc., Billerica, Massachusetts). Structural MR images were acquired using a 2D Rapid Imaging with Refocused Echoes (RARE) pulse sequence with the following parameters: effective echo time (TE_{eff}): 30 ms, RARE factor: 8. In-plane resolution: 100 µm x 100 µm, slice thickness: 300 µm and receiver bandwidth: 46875 Hz. The repetition time (TR) and the number of acquired slices were varied for two pairs of WT/KO mice in order to achieve greater slice coverage along the rostro-caudal axis (TR: 4000 ms to 4750 ms, number of slices: 40 to 50). The number of averages was varied to optimize total scan time for mouse imaging under gas anesthesia. Mice were euthanized at the end of the experiment.

Volumetry of lateral ventricles and total brain

The ventricles in each structural MRI scan were manually segmented by a separate researcher blind to animal genotypes using the ITK-SNAP software (www.itksnap.org).[26] While each ventricle was segmented separately, the volumes of both lateral ventricles were pooled together for all statistical analyses to account for the presence of fused lateral ventricles in several of the mutant mice. Q-Q plots and Levene's tests for both datasets indicate the data are normally distributed and variances are homogenous. Statistical analyses were performed by another independent researcher using R version 4.1.2 with Companion to Applied Regression package version 3.0, SPSS, and Tidyverse version 1.3.1 software.

Identification of regions of interest with reduced local volume

An image registration-based method was used to identify brain regions, at the voxel level, with significant local volume difference between WT and mutant mice, as described in Zha *et al.*[27] Briefly, a minimum deformation template was generated from the whole mouse population used in the current study, producing non-linear transformations mapping each scan into a common space. Voxel-level Jacobian determinants of the non-linear transformations were then calculated and used as a measure of the local volume difference between the average minimum deformation template and each individual mouse image. Voxel-level statistical analyses were performed using

RMINC version 1.5.3.0 software and statistical results were corrected for multiple comparisons using the false discovery rate method with a threshold of 10%. Regions in each individual scan for which local volumes differed significantly between WT and mutant mice were identified and analyzed. As well, brain regions in the mutant mice showing evidence of reduced volume were referenced to the Allen mouse brain atlas to identify more specific neuroanatomical areas and nuclei in mice that displayed reduced volume.

Data availability

Supplementary table 1 includes all raw data obtained in the cohort study and describes a comprehensive clinical description of each participant, as well as sums and averages of each phenotype for the cohort as a whole. Raw data concerning *in vitro* cell experiments and *in vivo* animal experiments were generated at the Montreal Neurological Institute of McGill University. Derived data supporting the findings of this study are available upon reasonable request from the corresponding author.

Results

Cohort Study

Our cohort consists of 15 individuals with biallelic *DENND5A* variants coming from 14 families with 21 unique variants. Females make up 60% of the cohort and the average age at the time of the last clinic visit from which answers to questionnaires were based upon was 9 years (*SD* = 4.8). Seven individuals are homozygous for *DENND5A* variants and, for the first time, we report eight individuals with compound heterozygous *DENND5A* variants exhibiting phenotypic overlap. Six members of the cohort were reported to have at least one additional variant flagged as potentially pathogenic, but the only gene with a variant of uncertain significance or potential pathogenicity that all individuals had in common was *DENND5A*. Table 1 summarizes each person in the cohort, including their *DENND5A* variant(s) and allele frequencies obtained from the gnomAD v2.1.1 dataset (https://gnomad.broadinstitute.org), and the presence (+) or absence (-) of the six most commonly reported phenotypes. None of the *DENND5A* variants present in the cohort were found in the homozygous state among 140,000 individuals on gnomAD, a

database that removes individuals affected by severe pediatric disease, indicating that biallelic pathogenic variants are incompatible with normal development. A schematic of human DENND5A protein along with the loci of all variants is shown in Figure 1A. Nineteen of the variants are found in the coding sequence with an additional two intronic variants located in splice sites (c.950-20_950-17delTTTT and c.2283+1G>T). The coding variants span the length of the protein including six in the DENN domain, two in the RUN1 domain, four in the PLAT domain, three in the RUN2 domain, and four in presumptive linker regions between the folded modules.

Supplementary table 1 provides comprehensive phenotypic data for each member of the cohort resulting from clinical evaluations by their physicians. “0” indicates a phenotype was not reported, “1” indicates a phenotype was documented to be present, and a cell left blank means its presence is unknown. The results of the study revealed the most frequently reported phenotypes observed in individuals with biallelic *DENND5A* variants are global developmental delay (93%), seizures (87%), ventriculomegaly (71%), hypotonia (67%), corpus callosum volume loss (64%), and microcephaly (60%; Fig. 1B).

Failure to meet key behavioral developmental milestones was almost universal in the cohort, evidenced by the fact that all but one exhibited global developmental delay. Most members of the cohort are nonverbal or are limited to single-word speech, and eye contact is observed in approximately half the cohort. Motor skill development was also delayed; four individuals can walk without support, and six are able to reach for and grasp objects. Seizure activity was reported in 13 individuals, with an age of onset averaging 3.2 months and all occurring within the first year of life. Most seizure activity was described as infantile spasms or tonic clonic seizures occurring multiple times per day. Seizures were controlled in only three cases. Abnormal MRIs were reported for all seven homozygous as well as for six compound heterozygous individuals. One compound heterozygous cohort member did not undergo neuroimaging for clinical purposes. Not all MR images were available but four MRIs from compound heterozygous individuals and two from homozygous individuals were made available and are presented in Figure 2. Notably, ventriculomegaly was present in 10 individuals, the extent of which ranges from mild to profound lateral ventricle enlargement as exemplified in the

presented MR images (Fig. 2). Additionally, nine and seven individuals have a reduction in corpus callosum and cerebral cortex volume, respectively.

Several common structural characteristics, muscular problems, and other non-neurological comorbidities were observed in the cohort. Microcephaly was among the most prevalent structural characteristics, but macrocephaly was also observed, perhaps as a secondary consequence of ventriculomegaly. In addition, most individuals had documented dysmorphic facial features; these include small chin, prominent nose, long eyelashes, full cheeks, and high palate, among others. The reports also commonly revealed central hypotonia and peripheral hypertonia, often accompanied by hyperreflexia, spastic tetraplegia, and/or clonus. Finally, chronic constipation, recurrent aspiration, oropharyngeal dysphagia, and episodes of oxygen desaturation each occur in at least half of the members of the cohort. These symptoms may be secondary to neurological dysfunction, as the smooth and skeletal muscles responsible for these phenotypes require extensive neuromuscular innervation.

Interestingly, phenotypic differences across several categories were observed between genotypes. Homozygous cohort members presented with structural brain abnormalities more frequently and with more severity than their compound heterozygous counterparts. Most remarkably, compared to compound heterozygotes, ventriculomegaly was approximately twice as frequent in homozygous individuals and appears to be more severe (Figs. 1B, 2). In addition, microcephaly was also approximately twice as frequent in homozygous compared to compound heterozygous cohort members (Fig. 1B), with average orbitofrontal circumference percentile rankings of 10% and 38%, respectively. In contrast, a reduction in corpus callosum volume was found in approximately equal proportions between the two types of genotypes (Fig. 1B), but the relative severity of the phenotypes again appears more pronounced in homozygous cohort members (Fig. 2).

Influence of variants on protein structure

To understand how *DENND5A* variants may be pathogenic, we modelled the structures of wild-type DENND5A as well as DENND5A protein with all missense mutations. As full-length DENND5A protein has not been crystallized, we used a DENND5A structure predicted by AlphaFold, an open-source homology- and artificial intelligence-based protein modelling

system.[28] Figure 3 shows a spacefill model of DENND5A with all missense variants highlighted in the structure. Each missense variant was analyzed separately using DynaMut, a system developed to analyze the impact of mutations on protein dynamics and stability, to assess DENND5A structural integrity.[29] Because most variants lie on the surface of the DENND5A molecule, no missense mutation is predicted to result in significant overall structural damage. However, the fact that these pathogenic missense residues lie on the outer molecular surface suggests vital inter- and/or intra-molecular interactions are altered by the amino acid substitutions.

Of the seven frameshift and nonsense variants, three result in stop codons located more than 50-55 nucleotides upstream of an exon-exon junction and are thus predicted to undergo nonsense-mediated mRNA decay. The remaining variants are presumed to result in a truncated and/or misfolded DENND5A protein.

Influence of variants on protein expression

To test which variants result in altered protein expression, *DENND5A* constructs with a N-terminal Flag tag and all coding sequence variants were generated, expressed in mammalian cells, and lysates were examined for DENND5A expression (Fig. 4A). Most variants express at or near wild type levels, consistent with structural analyses predicting no drastic alterations to structural integrity. Exceptions were found for some frameshift and nonsense variants. For example, protein products of approximately 20 kDa in size would be expected for truncating variants D173Pfs*8 and K205X, but the lack of detectable DENND5A when these constructs were overexpressed indicates potential misfolding and therefore a decrease in protein stability and subsequent degradation. All other truncating variants appeared at their predicted molecular weights, albeit with K850Sfs*11 and K1007Efs*10 expressing at reduced levels compared to WT, again indicating some level of protein instability.

We next sought to understand if variants in *DENND5A* influence its endogenous expression in cells derived from affected individuals. An iPSC line AIW001-02 derived from a healthy donor was edited to knockout DENND5A expression and cells were differentiated into NPCs along with iPSCs derived from one compound heterozygous (K485E/R710H) and two homozygous (D541G and Q1271Rfs*67) individuals. All cells express the neural precursor marker Nestin

after differentiation, confirming the identity of the cells as NPCs (Supplementary Fig. 2). The compound heterozygous individual (K485E/R710H) demonstrated DENND5A protein expression at approximately half the levels of WT, and homozygous cells (K205X and K850Sfs*11) express no detectable DENND5A protein (Fig. 4B). K205X is predicted to undergo nonsense-mediated mRNA decay, but our DENND5A antibody recognizes a region of the protein more C-terminal to the stop codon. mRNA levels were thus measured, but RT-qPCR data revealed that all cells derived from cohort members express DENND5A mRNA near control levels (Supplementary Fig. 3A).

Lymphoblasts from a healthy donor as well as from two homozygous cohort members were collected and immortalized with Epstein-Barr virus to establish lymphoblastoid cell lines. DENND5A protein expression was significantly reduced in both patient-derived cell lines compared to control cells (Fig. 4C), whereas in overexpression experiments these mutations expressed near WT levels (Fig. 4A). A downward shift was observed in the DENND5A band corresponding to D541G for an unknown reason, potentially implying a posttranslational modification or splice variant. An upward shift was observed for Q1271R*67; this finding was expected as the frameshift results in 17 mutant residues in the *DENND5A* coding sequence and an additional 49 residues resulting from the frameshift that allows for translation from the 3' untranslated region, resulting in a longer transcript than WT. Consistent with our RT-qPCR results in NPCs, we find that *DENND5A* RNA levels poorly correlate with protein expression, as we again found no significant difference in *DENND5A* mRNA levels between control and patient cells (Supplementary Fig. 3B).

Influence of variants on cell self-renewal

Loss of DENND5A has previously been shown to affect proper cell division.[20] To understand the potential effects that *DENND5A* variants have in the context of early development at the cellular level, we examined the ability of cells to divide symmetrically in neurosphere formation assays. Symmetric cell division results in two identical daughter cells and is an essential component of early cortical development, where the developing brain expands a pool of progenitor cells surrounding the developing ventricles that eventually populate the cortex. Alterations in this cell self-renewal process in NPCs has previously been shown to cause ventriculomegaly and dysgenesis of the cerebral cortex.[30] NPCs divide symmetrically and form clusters of cells in

suspension called neurospheres when cultured in a dish lacking a basement membrane coating such as laminin or Matrigel. After seeding a small number of cells per well and allowing the cells to grow over two weeks, we found that WT NPCs consistently form approximately 10 neurospheres of at least 50 µm in diameter per well (Fig. 5A/B). In contrast, disruption of DENND5A resulted in significant dysregulation of symmetric cell division. DENND5A KO NPCs failed to form any neurospheres, as did the cells derived from two cohort members (K485E/R710H and K205X). Surprisingly, the third patient-derived cell line (K850Sfs*11) formed more and larger neurospheres compared to WT (Fig. 5A/B). The reason for excess cell division in one cell line in which *DENND5A* is mutated and no cell division in the others is unknown, but may reflect that the KO, K205X and K485E/R710H cells have mutations that lead to loss of function, whereas K850Sfs*11 leads to a toxic gain of function. Regardless, in all cases the carefully controlled process of symmetric cell division is affected.

A DENND5A knockin mouse displays phenotypes seen in the human cohort

To assess causality between structural brain phenotypes and pathogenic biallelic *DENND5A* variants, a CRISPR/Cas9 knockin mouse model was generated with the two-nucleotide deletion c.517_518delGA/p.D173Pfs*8 found in one of the original DENND5A cohort members identified by Han *et al.*[9] and that is conserved in the mouse *DENND5A* sequence (Fig. 6A-B). Immunoblotting confirmed that full-length DENND5A protein is not expressed in homozygous knockin mice (Fig. 6C); however, as in the case of K205X patient-derived cells, our DENND5A antibody has an epitope recognizing a region more C-terminal to the stop codon. We thus measured *DENND5A* mRNA via RT-qPCR and a Welch's t-test revealed a significant reduction in expression levels in mutant mouse brains compared to WT ($t(13.4) = 2.20$, $P = 0.046$; Fig. 6D), suggesting some degree of nonsense-mediated RNA decay. Moreover, DENND5A protein with this mutation and a N-terminal Flag tag is completely degraded when overexpressed in HEK-293T cells.

Using sectioning and hematoxylin and eosin staining as well as through manual segmentation of the lateral ventricles based on high resolution 7T MRI scans, we observed that the mutant mice displayed ventriculomegaly (Fig. 6E/F). However, variability in lateral ventricular volume was

large and thus the effect of increased ventricular volume in homozygous mutant mice did not reach statistical significance (M_{WT} = 4824 mm^3, SD_{WT} = 1657 mm^3; M_{Mut} = 6234 mm^3, SD_{Mut} = 2734 mm^3; $t(14) = -1.25$, $P = .233$; Fig. 6G). Analysis of mouse structural MRI data did demonstrate that homozygous mutant mice had significantly smaller brains relative to WT mice (M_{WT} = 1.06, SD = 0.0811; M_{Mut} = 0.945, SD = 0.0302; $t(14) = 3.82$, $P = 0.002$; Fig. 6H).

A minimum deformation template representing the average anatomy of all scans from WT and mutant mice was generated, and regions with local volume differences between WT and homozygous mutant mice were identified using voxel-based statistics with a false discovery rate threshold of 10% (Fig. 7). Neuroanatomical regions showing the highest degree of volume difference between WT and homozygous mutants are shown in blue in Figure 7 and listed in Supplementary Table 2. Notably, members of our human imaging cohort also had abnormalities reported in several of the neuroanatomical regions identified as having reduced volume in the mice. In particular, areas with reductions in brain volume found in both mice and humans included the corpus callosum, cerebral cortex, cerebellum, basal ganglia, and thalamus. Interestingly, we see no evidence of spontaneous seizures in the mice, supporting the notion that the primary deficit resulting from DENND5A dysfunction is one of development.

Discussion

Our study reveals that pathogenic *DENND5A* variants result in a distinct form of EE. Evidence for the pathogenic nature of *DENND5A* variants is further shown through the introduction of biallelic *DENND5A* variants into a knockin mouse with an otherwise genetically similar background. In *DENND5A* EE, we believe that altered development results in seizure activity, rather than the reverse scenario in which seizures alter neurodevelopment. Indeed, two cohort members were not reported to have seizures. However, although seizures may be secondary to developmental effects, there is still value in attempting to control seizures pharmacologically. Alterations in neurodevelopment can lead to improper ratios of excitatory and inhibitory neurons and/or an improper number and positioning of neurons, and seizure activity will still be detrimental and can exacerbate symptoms. In fact, there are two cohort members who reportedly regressed in language development after experiencing a seizure, and one also regressed in motor abilities. Behavioral treatments may also benefit individuals with biallelic *DENND5A* variants.

Early intensive behavioral interventions that incorporate applied behavior analysis, an evidence-based treatment often recommended for children with autism spectrum disorder, have been shown to result in modest but clinically significant improvements in children with Rett syndrome[31] and Angelman syndrome,[32] two single-gene disorders with developmental phenotypes overlapping with *DENND5A*-linked disease. It is unknown if similar treatments would make observable differences in *DENND5A* EE, but future studies may explore this possibility if more individuals are identified, especially among those exhibiting fewer abnormalities in brain morphology.

The most frequently reported anatomical brain abnormalities reported in our cohort are ventriculomegaly and reduced corpus callosum volume. These abnormalities were reproduced in the homozygous mutant mice, providing confidence that pathogenic biallelic *DENND5A* variants are linked to this cluster of phenotypes. While there is variability in ventricle volumes between mice, this is similar to humans in which 71% of our cohort had documented ventriculomegaly with a wide range of severity. We also have not observed spontaneous seizure activity in any of the *DENND5A* mutant mice. Based on this observation, we can hypothesize that the pathogenic nature of biallelic *DENND5A* variants in humans is therefore primarily due to altered neurodevelopment rather than seizures.

The reduced volume of the whole brain as well as within specific brain regions in both humans and mutant mice is likely a result of neuronal dysgenesis. Very early in development, a tightly controlled process of symmetric and asymmetric cell division must occur to provide the developing brain with enough neural progenitor cells and, later, neurons.[33] When the cell self-renewal process is disrupted, ventriculomegaly and thinning of the cerebral cortex is observed.[30] We have demonstrated that the NPC self-renewal process in culture is grossly impaired in *DENND5A* KO and patient-derived cells, where most are unable to symmetrically divide at all and one patient cell line resulted in excessive cell self-renewal compared to WT. This result is consistent with previous studies showing DENND5A is required for proper cytokinesis, and a lack of DENND5A arrests the cell cycle in metaphase and ultimately results in cell death.[20] The reason behind homozygous K850Sfs*11 variants resulting in excessive cell self-renewal is unclear; however, it is reasonable to imagine that a developing brain with an overly large pool of progenitor cells could lead to a similar developmental result. An excess number of progenitor

cells would give rise to an excess number of newborn neurons migrating to the cortex, which may ultimately undergo apoptosis due to their inappropriate number and timing, resulting in the lack of necessary trophic support for neuron survival.

An individual's genotype and the specific allelic combination of *DENND5A* variants may contribute to overall disease severity. We observed the general pattern that individuals homozygous for *DENND5A* variants, independent of the type of variant, display phenotypes more frequently and to an apparently more severe degree, although statistical power to confirm this finding could not be achieved due to the small cohort size. For example, homozygous individuals exhibited the most acute cases of ventriculomegaly and corpus callosum volume reduction based on MRI scans. In contrast, both phenotypes are less pronounced in compound heterozygous MRIs, and are not reported at all in the individual with DENND5A variants K485E/R1159W.

It is worth emphasizing that the individual with genotype K485E/R1159W does not present with any of the hallmark phenotypes of *DENND5A*-related DEE. Despite sharing a variant (K485E) with another unrelated cohort member (K485E/R710H) that presents with all of the hallmark phenotypes, R1159W on their second allele may be a benign variant or have a comparatively mild developmental consequence, effectively making this person heterozygous for a pathogenic DENND5A variant. The specific impacts that R710H and R1159W have on DENND5A protein function requires further study to corroborate this finding.

It is plausible that some cases of DENND5A EE are present among other cohorts, such as in autism spectrum disorder (ASD) or pseudo-TORCH (Toxoplasmosis, Other agents, Rubella, Cytomegalovirus, and Herpes Simplex) syndrome. ASD is an umbrella diagnosis that encompasses a wide variety of developmental outcomes, primarily relating to sensory perception and social behavior, and is therefore believed to be caused by a multitude of genetic and/or environmental factors. It is possible that individuals with biallelic *DENND5A* variants, especially milder cases such as the three in our cohort who are in fact diagnosed with ASD, are part of the one in 160 children with ASD globally.[34] In addition, pseudo-TORCH syndrome is diagnosed when the hallmark clinical features of TORCH syndrome – which highly overlap with clinical features of *DENND5A* EE including ventriculomegaly, seizures, and microcephaly – are present but there is no evidence of an intra-uterine infectious origin.[35] However, no genetic data is

available regarding the known pseudo-TORCH patients to our knowledge, and it is unknown if *DENND5A* variants are behind any of these cases.

Physicians encountering infants and children with global developmental delay accompanied by hallmark features identified in this report such as seizures, ventriculomegaly, hypotonia, reduced corpus callosum volume, and/or microcephaly should consider screening for *DENND5A* variants and referring the families to genetic counseling. We also support the gene-disease assertion for *DENND5A* variants to be updated to "strong", thus allowing compelling variants in this gene to be classified as "Likely Pathogenic" according to ClinGen guidelines. The identification of additional *DENND5A* EE cases will prove valuable for future clinical and biological studies and thus improved treatment options and prognostic information for health care providers and families alike.

Acknowledgements

We would like to acknowledge all cohort members in this study, their families, and treating clinicians for their participation.

The views expressed are those of the author(s) and do not reflect the official policy of the Department of the Army, the Department of Defense or the U.S. Government.

Participant 10 was recruited as part of the German-Jordanian Autosomal Recessive Intellectual Disability project (GeJo-ARID) funded by the German Academic Exchange Service (DAAD) as part of the German-Arab Transformation Program Line4 (Project-ID 57166498).

The content is solely the responsibility of the authors and does not necessarily represent the official views of the National Institutes of Health.

Funding

This work was funded by a Foundation Grant from the Canadian Institutes of Health Research to PSM, and a grant from the Alain and Sandra Bouchard Foundation for Intellectual Disabilities to PSM and TMD.

This work was also supported by the King Salman Center for Disability Research through Research Group no RG-2022-010 (FSA).

This work was also performed under the Care4Rare Canada Consortium funded by Genome Canada and the Ontario Genomics Institute (OGI-147), the Canadian Institutes of Health Research, Ontario Research Fund, Genome Alberta, Genome British Columbia, Genome Quebec, and Children's Hospital of Eastern Ontario Foundation (DC, ESYG, MO).

Research reported in this manuscript was also supported by the NIH Common Fund, through the Office of Strategic Coordination/Office of the NIH Director under Award Number(s) [U01HG007672, U01HG007943] (HC).

Competing interests

KMc is employed by GeneDx, LLC. All other authors report no conflicts of interest.

Supplementary material

Supplementary material is available at *Brain* online.

Appendix 1

Members of the Undiagnosed Diseases Network include, Maria T. Acosta, Margaret Adam, David R. Adams, Pankaj B. Agrawal, Mercedes E. Alejandro, Justin Alvey, Laura Amendola, Ashley Andrews, Euan A. Ashley, Mahshid S. Azamian, Carlos A. Bacino, Guney Bademci, Eva Baker, Ashok Balasubramanyam, Dustin Baldridge, Jim Bale, Michael Bamshad, Deborah Barbouth, Gabriel F. Batzli, Pinar Bayrak-Toydemir, Anita Beck, Alan H. Beggs, Edward Behrens, Gill Bejerano, Jimmy Bennet, Beverly Berg-Rood, Raphael Bernier, Jonathan A. Bernstein, Gerard T. Berry, Anna Bican, Stephanie Bivona, Elizabeth Blue, John Bohnsack, Carsten Bonnenmann, Devon Bonner, Lorenzo Botto, Brenna Boyd, Lauren C. Briere, Elly Brokamp, Gabrielle Brown, Elizabeth A. Burke, Lindsay C. Burrage, Manish J. Butte, Peter Byers, William E. Byrd, John Carey, Olveen Carrasquillo, Ta Chen Peter Chang, Sirisak

Chanprasert, Hsiao-Tuan Chao, Gary D. Clark, Terra R. Coakley, Laurel A. Cobban, Joy D. Cogan, F. Sessions Cole, Heather A. Colley, Cynthia M. Cooper, Heidi Cope, William J. Craigen, Andrew B. Crouse, Michael Cunningham, Precilla D'Souza, Hongzheng Dai, Surendra Dasari, Mariska Davids, Jyoti G. Dayal, Matthew Deardorff, Esteban C. Dell'Angelica, Shweta U. Dhar, Katrina Dipple, Daniel Doherty, Naghmeh Dorrani, Emilie D. Douine, David D. Draper, Laura Duncan, Dawn Earl, David J. Eckstein, Lisa T. Emrick, Christine M. Eng, Cecilia Esteves, Tyra Estwick, Marni Falk, Liliana Fernandez, Carlos Ferreira, Elizabeth L. Fieg, Paul G. Fisher, Brent L. Fogel, Irman Forghani, Laure Fresard, William A. Gahl, Ian Glass, Rena A. Godfrey, Katie Golden-Grant, Alica M. Goldman, David B. Goldstein, Alana Grajewski, Catherine A. Groden, Andrea L. Gropman, Irma Gutierrez, Sihoun Hahn, Rizwan Hamid, Neil A. Hanchard, Kelly Hassey, Nichole Hayes, Frances High, Anne Hing, Fuki M. Hisama, Ingrid A. Holm, Jason Hom, Martha Horike-Pyne, Alden Huang, Yong Huang, Rosario Isasi, Fariha Jamal, Gail P. Jarvik, Jeffrey Jarvik, Suman Jayadev, Jean M. Johnston, Lefkothea Karaviti, Emily G. Kelley, Jennifer Kennedy, Dana Kiley, Isaac S. Kohane, Jennefer N. Kohler, Deborah Krakow, Donna M. Krasnewich, Elijah Kravets, Susan Korrick, Mary Koziura, Joel B. Krier, Seema R. Lalani, Byron Lam, Christina Lam, Brendan C. Lanpher, Ian R. Lanza, C. Christopher Lau, Kimberly LeBlanc, Brendan H. Lee, Hane Lee, Roy Levitt, Richard A. Lewis, Sharyn A. Lincoln, Pengfei Liu, Xue Zhong Liu, Nicola Longo, Sandra K. Loo, Joseph Loscalzo, Richard L. Maas, Ellen F. Macnamara, Calum A. MacRae, Valerie V. Maduro, Marta M. Majcherska, May Christine V. Malicdan, Laura A. Mamounas, Teri A. Manolio, Rong Mao, Kenneth Maravilla, Thomas C. Markello, Ronit Marom, Gabor Marth, Beth A. Martin, Martin G. Martin, Julian A. Martínez-Agosto, Shruti Marwaha, Jacob McCauley, Allyn McConkie-Rosell, Colleen E. McCormack, Alexa T. McCray, Elisabeth McGee, Heather Mefford, J. Lawrence Merritt, Matthew Might, Ghayda Mirzaa, Eva Morava-Kozicz, Paolo M. Moretti, Marie Morimoto, John J. Mulvihill, David R. Murdock, Mariko Nakano-Okuno, Avi Nath, Stan F. Nelson, John H. Newman, Sarah K. Nicholas, Deborah Nickerson, Donna Novacic, Devin Oglesbee, James P. Orengo, Laura Pace, Stephen Pak, J. Carl Pallais, Christina GS. Palmer, Jeanette C. Papp, Neil H. Parker, John A. Phillips III, Jennifer E. Posey, Lorraine Potocki, Barbara N. Pusey, Aaron Quinlan, Wendy Raskind, Archana N. Raja, Genecee Renteria, Chloe M. Reuter, Lynette Rives, Amy K. Robertson, Lance H. Rodan, Jill A. Rosenfeld, Natalie Rosenwasser, Robb K. Rowley, Maura Ruzhnikov, Ralph Sacco, Jacinda B. Sampson, Susan L. Samson, Mario Saporta, C. Ron

Scott, Judy Schaechter, Timothy Schedl, Kelly Schoch, Daryl A. Scott, Prashant Sharma, Vandana Shashi, Jimann Shin, Rebecca Signer, Catherine H. Sillari, Edwin K. Silverman, Janet S. Sinsheimer, Kathy Sisco, Edward C. Smith, Kevin S. Smith, Emily Solem, Lilianna Solnica-Krezel, Rebecca C. Spillmann, Joan M. Stoler, Nicholas Stong, Jennifer A. Sullivan, Kathleen Sullivan, Angela Sun, Shirley Sutton, David A. Sweetser, Virginia Sybert, Holly K. Tabor, Cecelia P. Tamburro, Queenie K.-G. Tan, Mustafa Tekin, Fred Telischi, Willa Thorson, Cynthia J. Tifft, Camilo Toro, Alyssa A. Tran, Brianna M. Tucker, Tiina K. Urv, Adeline Vanderver, Matt Velinder, Dave Viskochil, Tiphanie P. Vogel, Colleen E. Wahl, Stephanie Wallace, Nicole M. Walley, Chris A. Walsh, Melissa Walker, Jennifer Wambach, Jijun Wan, Lee-kai Wang, Michael F. Wangler, Patricia A. Ward, Daniel Wegner, Mark Wener, Tara Wenger, Katherine Wesseling Perry, Monte Westerfield, Matthew T. Wheeler, Jordan Whitlock, Lynne A. Wolfe, Jeremy D. Woods, Shinya Yamamoto, John Yang, Guoyun Yu, Diane B. Zastrow, Chunli Zhao, Stephan Zuchner.

References

1. Berg AT, Cross JH. Towards a modern classification of the epilepsies? *Lancet Neurol*. May 2010;9(5):459-61. doi:10.1016/S1474-4422(10)70024-7

2. Kim HJ, Yang D, Kim SH, et al. Genetic and clinical features of SCN8A developmental and epileptic encephalopathy. *Epilepsy Res*. Dec 2019;158:106222. doi:10.1016/j.eplepsyres.2019.106222

3. Sadleir LG, Mountier EI, Gill D, et al. Not all SCN1A epileptic encephalopathies are Dravet syndrome: Early profound Thr226Met phenotype. *Neurology*. Sep 5 2017;89(10):1035-1042. doi:10.1212/WNL.0000000000004331

4. Zhang J, Kim EC, Chen C, et al. Identifying mutation hotspots reveals pathogenetic mechanisms of KCNQ2 epileptic encephalopathy. *Sci Rep*. Mar 16 2020;10(1):4756. doi:10.1038/s41598-020-61697-6

5. de Vries PJ, Howe CJ. The tuberous sclerosis complex proteins--a GRIPP on cognition and neurodevelopment. *Trends Mol Med*. Aug 2007;13(8):319-26. doi:10.1016/j.molmed.2007.06.003

6. Lux AL, Edwards SW, Hancock E, et al. The United Kingdom Infantile Spasms Study (UKISS) comparing hormone treatment with vigabatrin on developmental and epilepsy outcomes to age 14 months: a multicentre randomised trial. *Lancet Neurol*. Nov 2005;4(11):712-7. doi:10.1016/S1474-4422(05)70199-X

7. Bradshaw J, Steiner AM, Gengoux G, Koegel LK. Feasibility and effectiveness of very early intervention for infants at-risk for autism spectrum disorder: a systematic review. *J Autism Dev Disord*. Mar 2015;45(3):778-94. doi:10.1007/s10803-014-2235-2

8. Cioni G, Inguaggiato E, Sgandurra G. Early intervention in neurodevelopmental disorders: underlying neural mechanisms. *Dev Med Child Neurol*. Mar 2016;58 Suppl 4:61-6. doi:10.1111/dmcn.13050

9. Han C, Alkhater R, Froukh T, et al. Epileptic Encephalopathy Caused by Mutations in the Guanine Nucleotide Exchange Factor DENND5A. *Am J Hum Genet*. Dec 1 2016;99(6):1359-1367. doi:10.1016/j.ajhg.2016.10.006

10. Allaire PD, Marat AL, Dall'Armi C, Di Paolo G, McPherson PS, Ritter B. The Connecdenn DENN domain: a GEF for Rab35 mediating cargo-specific exit from early endosomes. *Mol Cell*. Feb 12 2010;37(3):370-82. doi:10.1016/j.molcel.2009.12.037

11. Zhang D, Iyer LM, He F, Aravind L. Discovery of Novel DENN Proteins: Implications for the Evolution of Eukaryotic Intracellular Membrane Structures and Human Disease. *Front Genet*. 2012;3:283. doi:10.3389/fgene.2012.00283

12. Marat AL, Dokainish H, McPherson PS. DENN domain proteins: regulators of Rab GTPases. *J Biol Chem*. Apr 22 2011;286(16):13791-800. doi:10.1074/jbc.R110.217067

13. Callebaut I, de Gunzburg J, Goud B, Mornon JP. RUN domains: a new family of domains involved in Ras-like GTPase signaling. *Trends Biochem Sci*. Feb 2001;26(2):79-83. doi:10.1016/s0968-0004(00)01730-8

14. Janoueix-Lerosey I, Jollivet F, Camonis J, Marche PN, Goud B. Two-hybrid system screen with the small GTP-binding protein Rab6. Identification of a novel mouse GDP dissociation inhibitor isoform and two other potential partners of Rab6. *J Biol Chem*. Jun 16 1995;270(24):14801-8. doi:10.1074/jbc.270.24.14801

15. Recacha R, Boulet A, Jollivet F, et al. Structural basis for recruitment of Rab6-interacting protein 1 to Golgi via a RUN domain. *Structure*. Jan 14 2009;17(1):21-30. doi:10.1016/j.str.2008.10.014

16. Fernandes H, Franklin E, Khan AR. Crystallization of an engineered RUN domain of Rab6-interacting protein 1/DENND5. *Acta Crystallogr Sect F Struct Biol Cryst Commun*. May 1 2011;67(Pt 5):556-60. doi:10.1107/S174430911100724X

17. Fernandes H, Franklin E, Jollivet F, Bliedtner K, Khan AR. Mapping the interactions between a RUN domain from DENND5/Rab6IP1 and sorting nexin 1. *PLoS One*. 2012;7(4):e35637. doi:10.1371/journal.pone.0035637

18. Wassmer T, Attar N, Harterink M, et al. The retromer coat complex coordinates endosomal sorting and dynein-mediated transport, with carrier recognition by the trans-Golgi network. *Dev Cell*. Jul 2009;17(1):110-22. doi:10.1016/j.devcel.2009.04.016

19. Bateman A, Sandford R. The PLAT domain: a new piece in the PKD1 puzzle. *Curr Biol*. Aug 26 1999;9(16):R588-90. doi:10.1016/s0960-9822(99)80380-7

20. Miserey-Lenkei S, Waharte F, Boulet A, et al. Rab6-interacting protein 1 links Rab6 and Rab11 function. *Traffic*. Oct 2007;8(10):1385-403. doi:10.1111/j.1600-0854.2007.00612.x

21. Anazi S, Maddirevula S, Faqeih E, et al. Clinical genomics expands the morbid genome of intellectual disability and offers a high diagnostic yield. *Mol Psychiatry*. Apr 2017;22(4):615-624. doi:10.1038/mp.2016.113

22. Sobreira N, Schiettecatte F, Valle D, Hamosh A. GeneMatcher: a matching tool for connecting investigators with an interest in the same gene. *Hum Mutat*. Oct 2015;36(10):928-30. doi:10.1002/humu.22844

23. Landrum MJ, Lee JM, Benson M, et al. ClinVar: improving access to variant interpretations and supporting evidence. *Nucleic Acids Res*. Jan 4 2018;46(D1):D1062-D1067. doi:10.1093/nar/gkx1153

24. Okita K, Matsumura Y, Sato Y, et al. A more efficient method to generate integration-free human iPS cells. *Nat Methods*. May 2011;8(5):409-12. doi:10.1038/nmeth.1591

25. Hauser S, Erzler M, Theurer Y, Schuster S, Schule R, Schols L. Establishment of SPAST mutant induced pluripotent stem cells (iPSCs) from a hereditary spastic paraplegia (HSP) patient. *Stem Cell Res*. Nov 2016;17(3):485-488. doi:10.1016/j.scr.2016.09.022

26. Yushkevich PA, Piven J, Hazlett HC, et al. User-guided 3D active contour segmentation of anatomical structures: significantly improved efficiency and reliability. *Neuroimage*. Jul 1 2006;31(3):1116-28. doi:10.1016/j.neuroimage.2006.01.015

27. Zha C, Farah CA, Fonov V, Rudko DA, Sossin WS. MRI of Capn15 Knockout Mice and Analysis of Capn 15 Distribution Reveal Possible Roles in Brain Development and Plasticity. *Neuroscience*. Jun 15 2021;465:128-141. doi:10.1016/j.neuroscience.2021.04.023

28. Jumper J, Evans R, Pritzel A, et al. Highly accurate protein structure prediction with AlphaFold. *Nature*. Aug 2021;596(7873):583-589. doi:10.1038/s41586-021-03819-2

29. Rodrigues CH, Pires DE, Ascher DB. DynaMut: predicting the impact of mutations on protein conformation, flexibility and stability. *Nucleic Acids Res*. Jul 2 2018;46(W1):W350-W355. doi:10.1093/nar/gky300

30. Geng A, Qiu R, Murai K, et al. KIF20A/MKLP2 regulates the division modes of neural progenitor cells during cortical development. *Nat Commun*. Jul 13 2018;9(1):2707. doi:10.1038/s41467-018-05152-1

31. Titlestad KB, Eldevik S. Brief Report: Modest but Clinically Meaningful Effects of Early Behavioral Intervention in Twins with Rett Syndrome-A Case Study. *J Autism Dev Disord*. Dec 2019;49(12):5063-5072. doi:10.1007/s10803-019-04185-9

32. Summers J. Neurodevelopmental outcomes in children with Angelman syndrome after 1 year of behavioural intervention. *Dev Neurorehabil*. 2012;15(4):239-52. doi:10.3109/17518423.2012.676101

33. Huttner WB, Kosodo Y. Symmetric versus asymmetric cell division during neurogenesis in the developing vertebrate central nervous system. *Curr Opin Cell Biol*. Dec 2005;17(6):648-57. doi:10.1016/j.ceb.2005.10.005

34. Elsabbagh M, Divan G, Koh YJ, et al. Global prevalence of autism and other pervasive developmental disorders. *Autism Res*. Jun 2012;5(3):160-79. doi:10.1002/aur.239

35. Vivarelli R, Grosso S, Cioni M, et al. Pseudo-TORCH syndrome or Baraitser-Reardon syndrome: diagnostic criteria. *Brain Dev*. Mar 2001;23(1):18-23. doi:10.1016/s0387-7604(00)00188-1

Figure Legends

Figure 1 DENND5A variant localization and phenotype distribution between genotypes. (A) Schematic representation of DENND5A protein and the localization of all *DENND5A* variants in the cohort. Intronic variants are listed as additions beneath the schematic. **(B)** The

total number (entire bar length) of DENND5A cohort members exhibiting each of the most frequently reported phenotypes. Each bar is further divided into the number of homozygous (dark gray) and compound heterozygous (light gray) individuals exhibiting each phenotype.

Figure 2 Biallelic DENND5A variants result in abnormal brain MRIs in all but one individual. Sagittal and axial views of all available MRIs of cohort members.

Figure 3 DENND5A protein modeling shows most missense variants lie on outer surface. Two views of a space-fill model of human DENND5A protein structure predicted by AlphaFold. Conserved protein modules are color-coded; green = DENN domain, purple = RUN1/PLAT tandem domains, and blue = RUN2 domain. Gray residues indicate non-conserved stretches of amino acids that link one conserved protein module to another. Residues impacted by missense variants in the cohort are highlighted in red.

Figure 4 *DENND5A* variants often result in altered protein expression. (A) WT and mutant FLAG-DENND5A expression 24h post-transfection in HEK-293T cells detected using an antibody recognizing FLAG. **(B)** DENND5A expression in WT, DENND5A KO, and patient NPCs detected using an antibody recognizing DENND5A. **(C)** DENND5A expression in control and patient lymphoblasts detected using an antibody recognizing DENND5A.

Figure 5 *DENND5A* variants result in altered cell self-renewal capacity in NPCs. (A) Representative field views of each condition after neurospheres were allowed to form for 14 days. Scale bar = 100 μm. **(B)** Quantification of the number of spheres with a diameter of at least 50 μm. Kruskal-Wallis test with Mann-Whitney U pairwise comparisons and Bonferroni corrections for multiple comparisons: * = $P < 0.05$, *** = $P < 0.0001$

Figure 6 A *DENND5A* knockin mouse model demonstrates features consistent with human cohort. (A) Alignment of human and mouse DENND5A nucleotides and amino acid residues show that the sequence is conserved between species. Highlighted nucleotides indicate the deletion introduced into the *DENND5A* mutant mice. Nucleotide numbers correspond to the respective coding sequence. **(B)** Sample chromatograms show that the homozygous mutant mice have a c.517_518delGA mutation. **(C)** Immunoblot of mouse brain lysate show a ~50% reduction of full-length DENND5A protein in heterozygous mice, and no detectable DENND5A protein in homozygous mutant mice. **(D)** RT-qPCR experiments show that mRNA expression of

DENND5A in mutant mouse brains is approximately 60% that of WT. Two-tailed *t*-test of log2 normalized expression values: * = $P < 0.05$. **(E)** H&E stains of WT and *DENND5A* mutant mouse brains show ventriculomegaly of the lateral ventricles. **(F)** *In vivo* mouse coronal, structural MRI scans showing manual segmentations of the lateral ventricles for WT and homozygous mutant mice. Blue crosshairs show the position of the selected axial and coronal image slices in Figure 6. L/R = left/right axis, H/F = head/foot axis, A/P = anterior/posterior axis. Green = left ventricle, red = right ventricle, blue = third ventricle, yellow = fourth ventricle. Scale bar = 1 cm. **(G)** Quantification of pooled lateral ventricle volumes for WT and mutant mice. **(H)** Normalized brain sizes measured via MRI. The bar plots show that *DENND5A* mutant mice have significantly smaller brains than WT mice.

Figure 7 DENND5A knockin mice show regions of significantly reduced brain volume. T-statistical maps, identified using high resolution *in vivo* mouse MRI, showing brain areas where mutant mice had reduced local volume compared to WT mice. Regions where mutant mice had decreased local volume compared to WT are highlighted in blue, with larger local volume differences in light blue. Regions where mutant mice had increased local volume compared to WT are highlighted in red. The slice location in the brain for each of the 36 slices demonstrated in the figure is shown with green lines overlaid on the sagittal mouse brain view in the top right corner of Figure 7.

Table 1 Demographic and phenotypic summary of DENND5A cohort members. Indicates participant sex and age, specific *DENND5A* variants and their population allele frequencies, the presence (+) or absence (-) of the most frequently identified phenotypes, as well as any additional flagged genetic variants in each individual.

Supplementary Figure 1 Phenotypic questionnaire that clinicians answered according to their patient's most recent clinic visit.

Supplementary Figure 2 WT, DENND5A KO, and patient-derived iPSCs differentiated to NPCs. All cell lines express the NPC marker Nestin. Scale bar = 10 μm.

Supplementary Figure 3 Relative *DENND5A* RNA expression in (A) NPCs and (B) lymphoblasts.

Supplementary Table 1 Complete dataset of phenotypes observed in the *DENND5A* cohort

Supplementary Table 2 Brain volume reductions in *DENND5A* knockin mice are consistent with human cohort Brain regions in which mutant mice have a reduction in local volume are also common regions in which DENND5A cohort members show abnormalities based on their brain MRI scans.

Table 1 DENND5A Cohort Summary

Patient	*DENND5A* zygosity	*DENND5A* variant(s)	Allele frequency	GDD[a]	Seizures	VM[b]	Hypotonia	Reduced CC volume[c]	Microcephaly	Other gene variants
M, 5-10y	Compound heterozygous	R698W N1017S	2.78×10^{-5} 1.59×10^{-5}	+	+	+	-	-	-	*CNOT3*
F, 5-10y	Compound heterozygous	K485E R710H	7.08×10^{-4} 5.17×10^{-5}	+	+	+	+	+	+	-
M, 15-20y	Homozygous	K205X	N/A	+	+	+	-	-	+	-
F, 5-10y	Homozygous	D541G	N/A	+	+	+	+	+	+	-
F, 5-10y	Homozygous	Q1271Rfs*67	N/A	+	+	+	-	-	+	-
F, 10-15y	Compound heterozygous	S455P A1245T	N/A 7.96×10^{-6}	+	+	-	-	+	-	*PEX1*, *CDC48*
M, 10-15y	Compound heterozygous	K485E R1159W	7.08×10^{-4} 9.20×10^{-5}	-	-	-	-	-	-	*HERC2*, *MYBPC3*
F, deceased 0-5y	Compound heterozygous	c.950-20_950-17delTTTT R1078Q	4.06×10^{-5} 2.62×10^{-4}	+	+	-	+	+	-	*TBCK*
F, 10-15y	Homozygous	K850Sfs*11	N/A	+	+	+	+	+	+	-
M, 0-5y	Compound heterozygous	R772X L1005M	3.19×10^{-5} N/A	+	+	-	+	-	+	CNV: 697 kb gain 6q25.3
M, 0-5y	Homozygous	S728fs*34	N/A	+	+	+	+	+	+	-
F, ?y	Homozygous	D173Qfs*8	N/A	+	+	+	+	+	-	-
F, ?y	Homozygous	D173Qfs*8	N/A	+	+	+	+	+	+	-
F, 15-20y	Compound heterozygous	c.2283+1G>T K1007Efs*10	N/A N/A	+	+	+	+	+	+	-
M, 5-10y	Compound heterozygous	T136R P955L	N/A 1.59×10^{-5}	+	-	unknown	+	unknown	-	*CACNA1C*

[a]GDD = global developmental delay

[b]VM = ventriculomegaly

[c]CC = corpus callosum

A

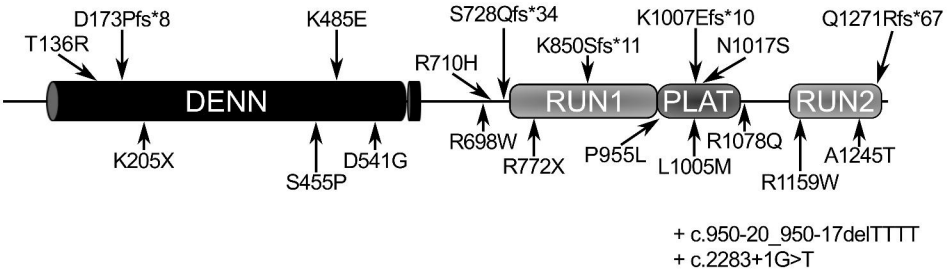

B

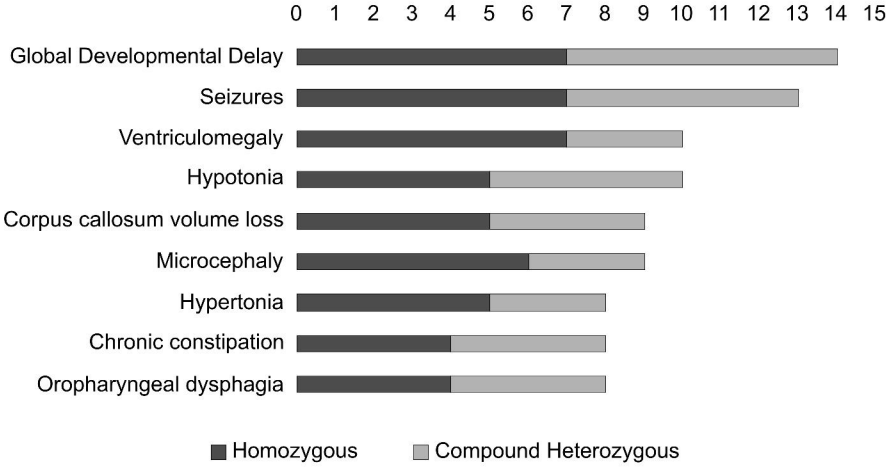

Banks et al., Fig. 1

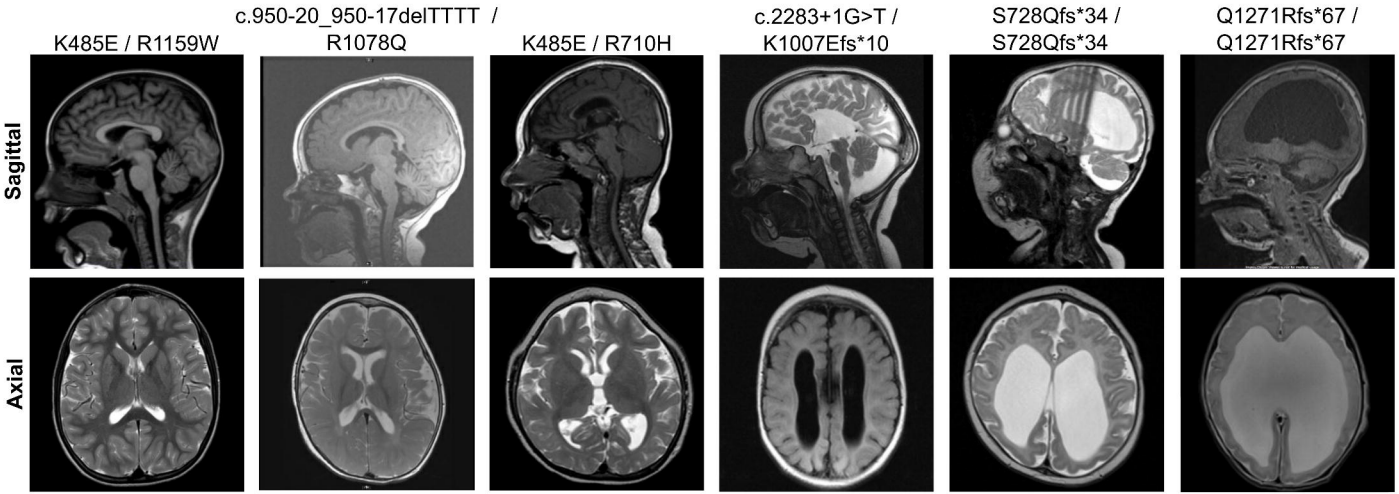

Banks et al., Fig. 2

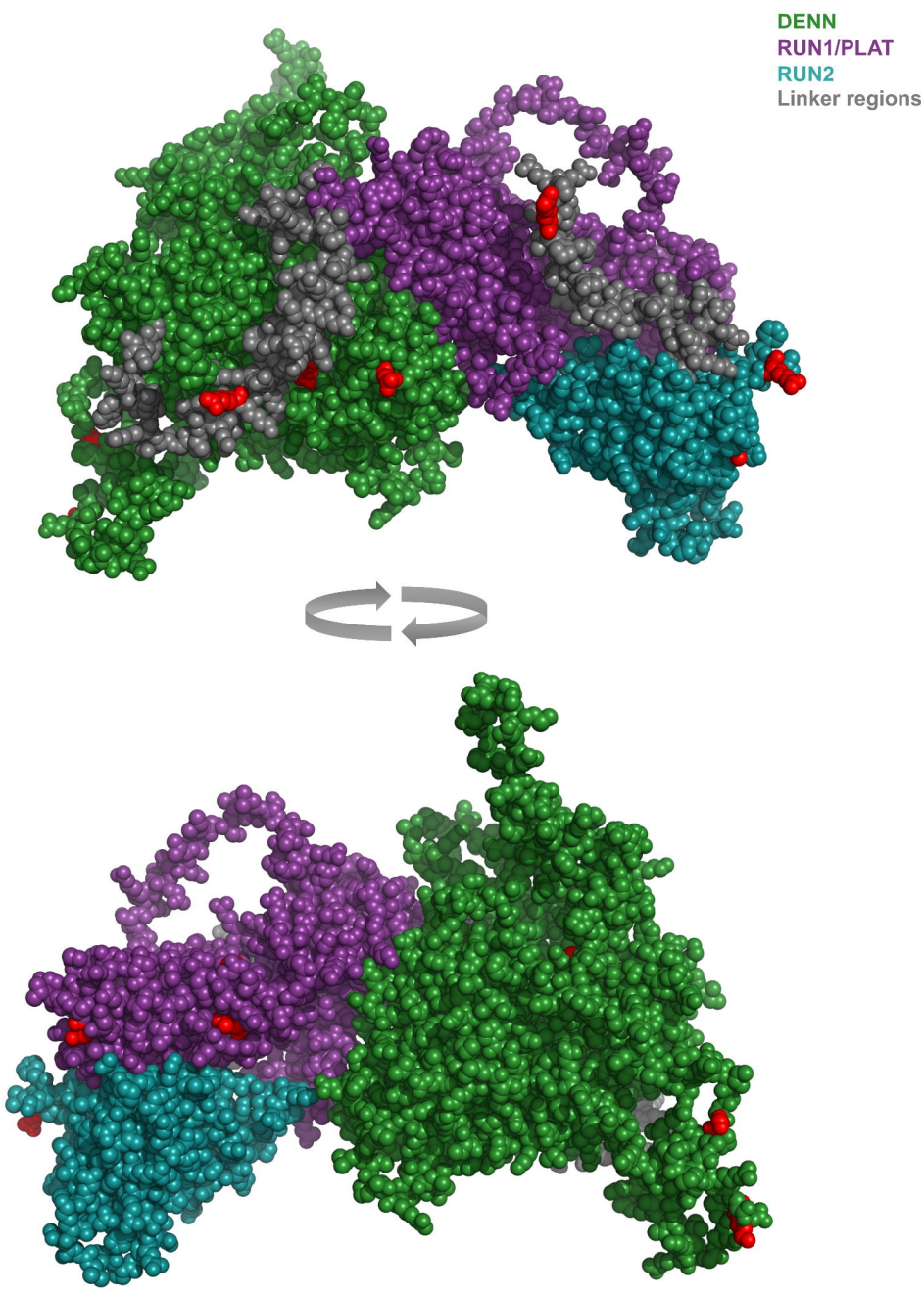

Banks et al., Fig. 3

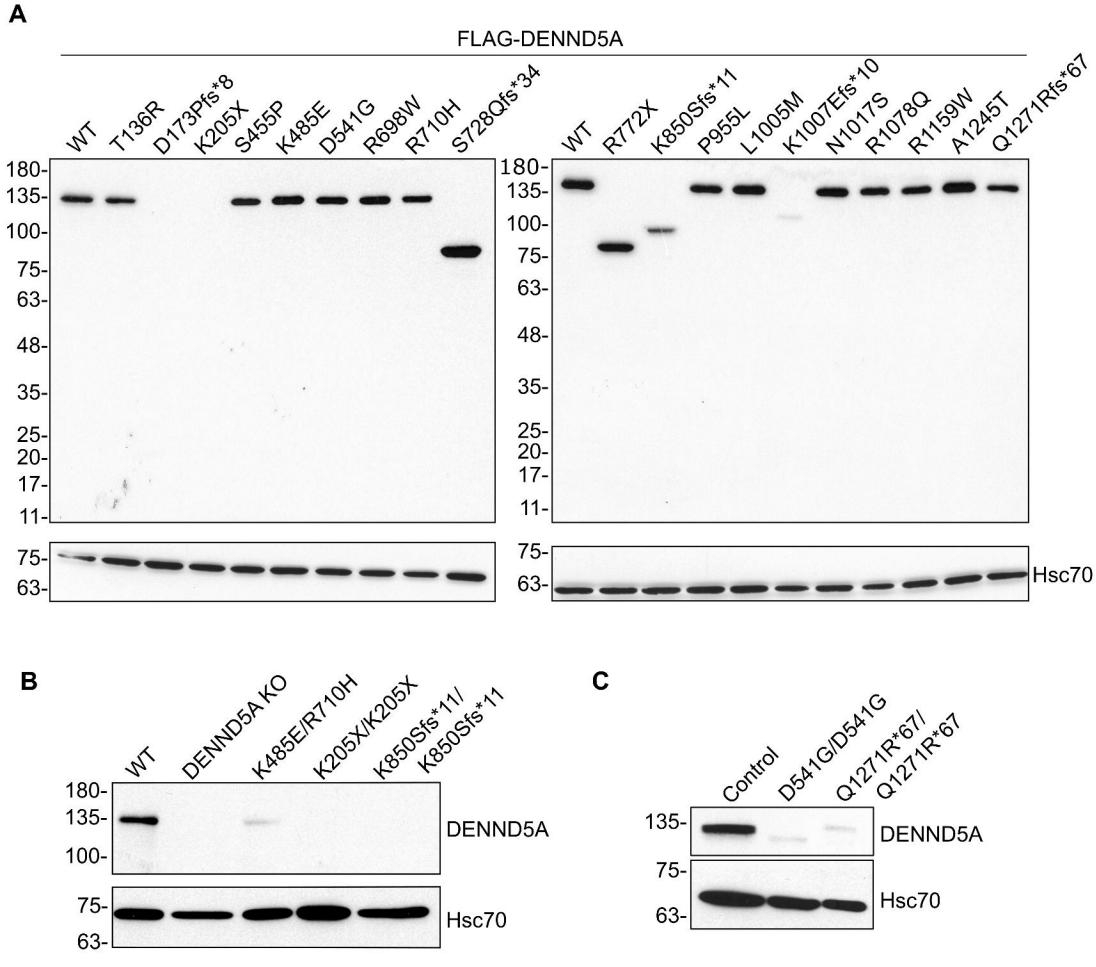

Banks et al., Fig. 4

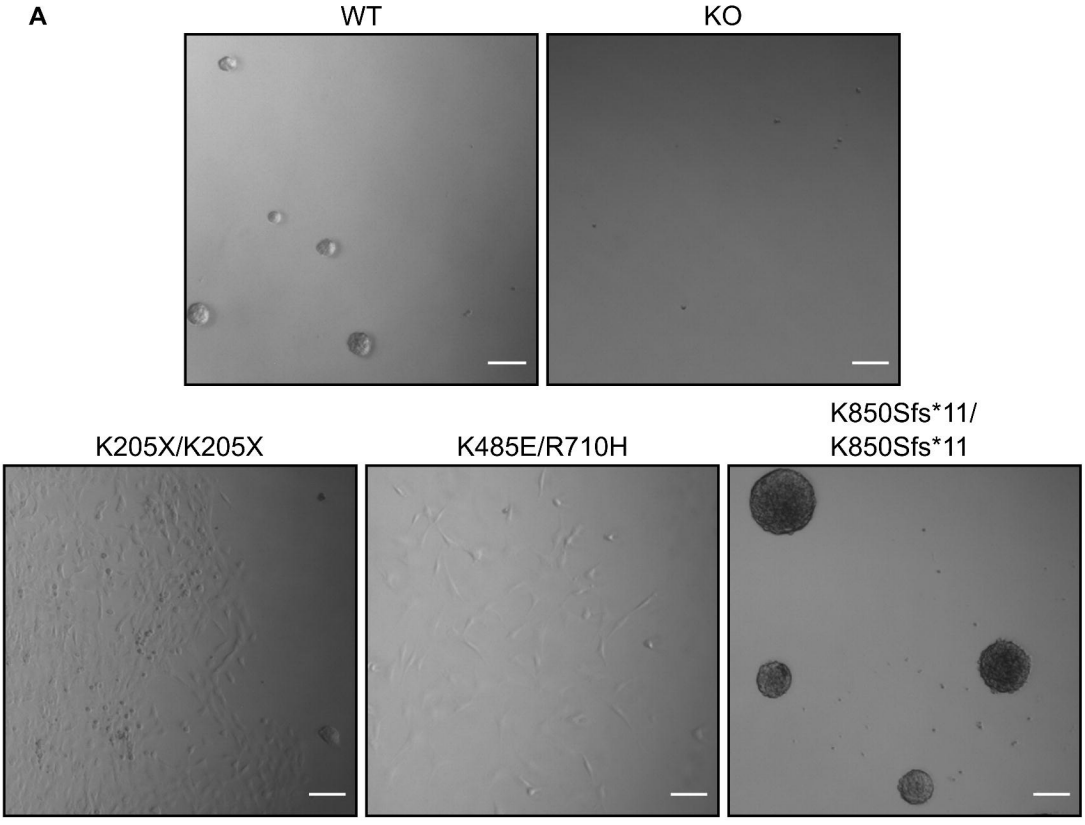

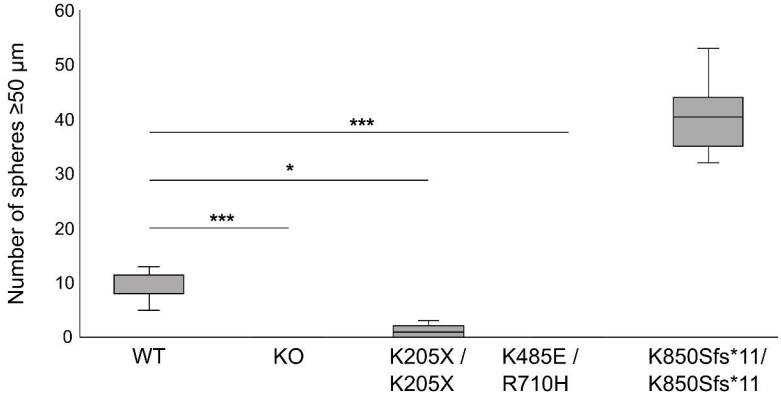

Banks et al., Fig. 5

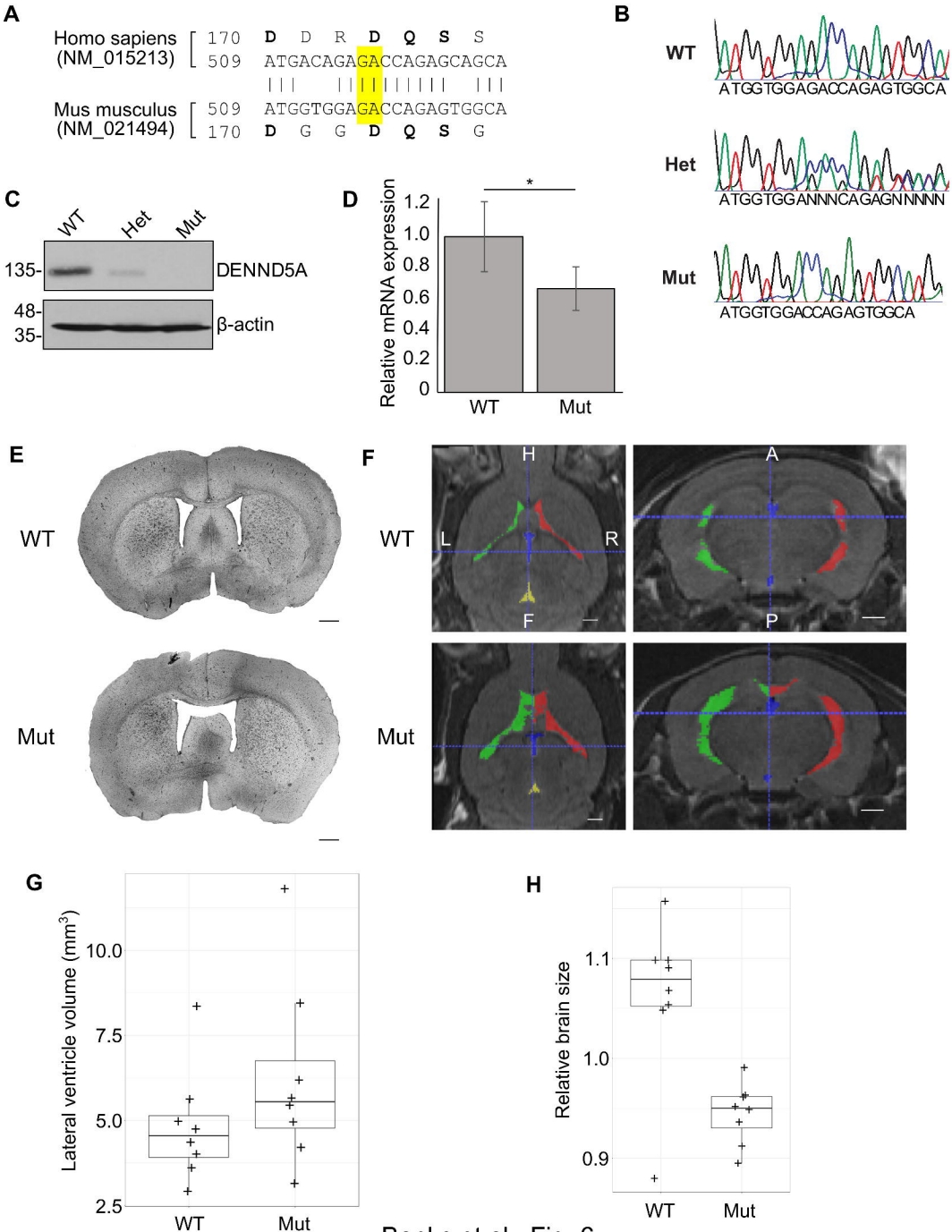

Banks et al., Fig. 6

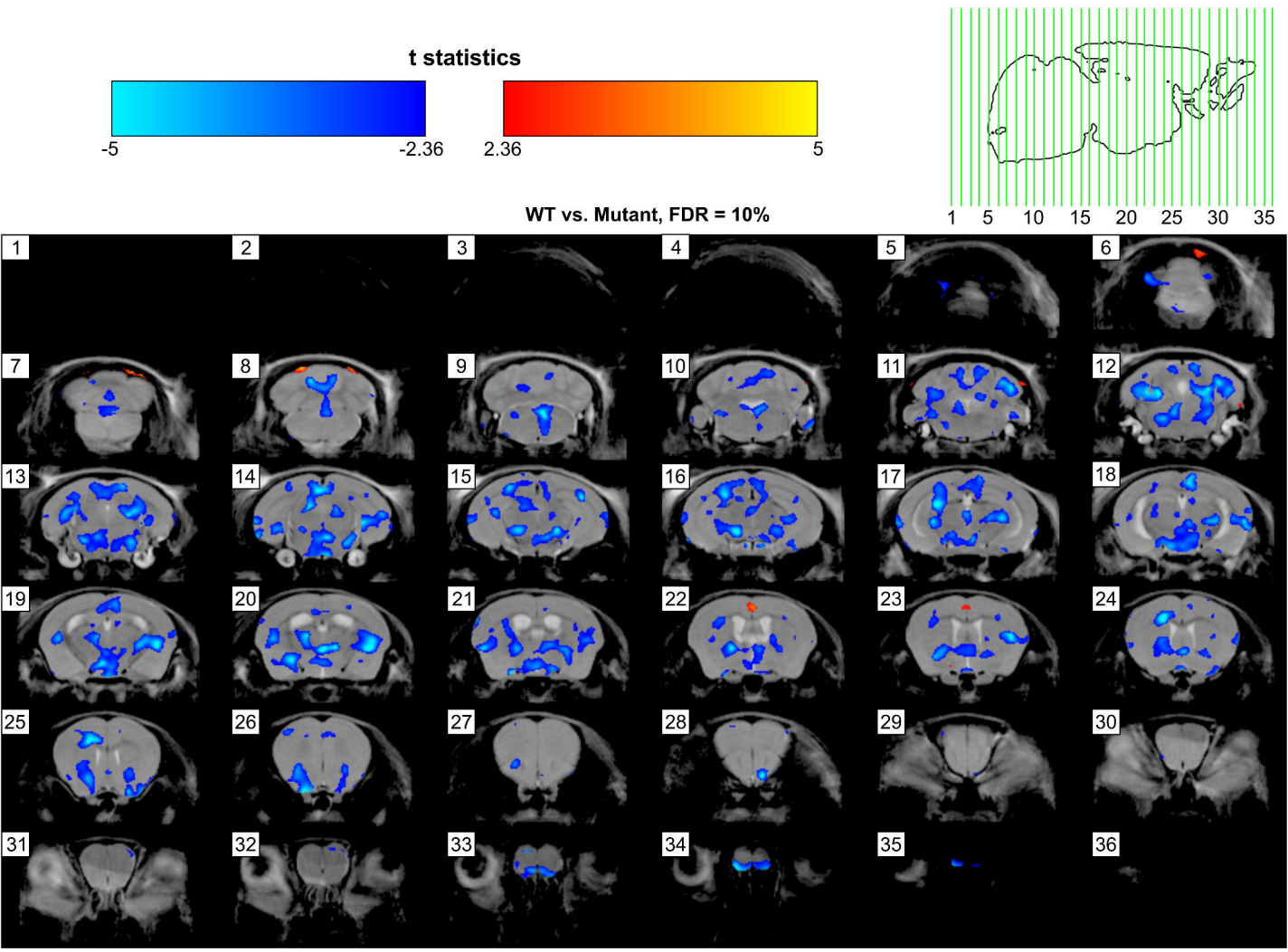

Banks et al., Fig. 7